PASJ: Publ. Astron. Soc. Japan **63**, 63–70, 2011 February 25

Astrometry of AGB Variables with VERA: Annual Parallax and the Orbit of SY Sculptoris in the Galaxy

Daisuke NYU,[1] Akiharu NAKAGAWA,[1] Makoto MATSUI,[1] Hiroshi IMAI,[1] Yoshiaki SOFUE[1] Toshihiro OMODAKA[1] Tomoharu KURAYAMA[1] Ryuichi KAMOHARA,[2] Tomoya HIROTA,[2,4] Mareki HONMA,[2,4] Katsunori M. SHIBATA,[2,4] Hideyuki KOBAYASHI,[3,5] Kenzaburo IWADATE,[5] and Takeshi MIYAJI[2]

[1]*Graduate School of Science and Engineering, Kagoshima University, 1-21-35 Kôrimoto, Kagoshima, Kagoshima 890-0065*

[2]*Mizusawa VLBI Observatory, National Astronomical Observatory of Japan, 2-21-1 Osawa, Mitaka, Tokyo 181-8588*

[3]*Department of Astronomy, Graduate School of Science, The University of Tokyo, 7-3-1 Hongo, Bunkyo-ku, Tokyo 113-0033*

[4]*Department of Astronomical Sciences, Graduate University for Advanced Studies, 2-21-1 Osawa, Mitaka, Tokyo 181-8588*

[5]*Mizusawa VLBI Observatory, National Astronomical Observatory of Japan, 2-12 Hoshigaoka, Mizusawa-ku, Oshu, Iwate 023-0861*

(Received 2009 February 14; accepted 2010 August 9)

Abstract

We report on the results of astrometric observations of H_2O masers toward a Mira variable, SY Sculptoris (SY Scl), with the VLBI Exploration of Radio Astrometry (VERA) from 2006 October to 2008 October. We determined that SY Scl's annual parallax is 0.75 ± 0.03 mas, corresponding to a distance of 1.33 ± 0.05 kpc. SY Scl is 1.3 kpc south of the Galactic plane and moves approximately south from the plane with a velocity of $63 \pm 2\,\mathrm{km\,s^{-1}}$ with respect to the LSR. From the present position and motion, we calculated SY Scl's orbit for the last 1 Gyr based on a parametrized model of the Galactic gravitational potential. SY Scl has an orbit as a member of the Galactic thick disk stars. Subtracting the averaged absolute proper motions of masers, we derived an internal motion of H_2O masers in SY Scl. The kinematics of the masers is consistent with motion in a single plane. The masers around SY Scl were found to be distributed in an area of 70 AU × 80 AU, corresponding to 15 times as large as the stellar photosphere diameter of 5 AU. Based on the measured distance and apparent magnitude of SY Scl, we find the absolute magnitude of SY Scl to be $M_K = -8.07 \pm 0.08$ mag. This is approximately consistent with the value of -8.09 ± 0.07 mag, which was derived from the Galactic Mira period–luminosity relation (2008, MNRAS, 386, 313).

Key words: astrometry — masers(H_2O) — stars: AGB and post-AGB — stars: individual(SY Sculptoris)

1. Introduction

Measurements of annual parallaxes for OH, SiO, and H_2O masers associated with Mira variables with the very long baseline interferometry (VLBI) technique promise accurate distance measurements. Especially, in the case where a source has such a high mass-loss rate that the circumstellar envelope affects its luminosity, the VLBI technique can be a powerful tool for measuring its distance instead of optical astrometry.

VLBI astrometric observations have been carried out with a fast antenna-switching method to obtain relative positions with respect to extragalactic reference sources (e.g., Shapiro et al. 1979). The results have yielded a position accuracy of 0.1 mas, or higher. In recent VLBI observations, annual parallaxes have been successfully measured for OH maser sources at 1.6 GHz (e.g., van Langevelde et al. 2000; Vlemmings et al. 2003), for CH_3OH maser sources at both 6.7 GHz and 12 GHz (e.g., Rygl et al. 2010), and for H_2O maser sources at 22 GHz (e.g., Kurayama et al. 2005) with the VLBA on the kiloparsec scale. The target volume is scaled up to the size of the Galaxy. Thus, the Hipparcos satellite and VLBI establish astrometric links between a large variety of celestial objects.

The VLBI Exploration of Radio Astrometry (VERA) is a Japanese VLBI array dedicated for a phase-referencing technique. VERA has four radio telescopes with dual-beam systems that enable us to simultaneously observe two adjacent ($\leq 2.^\circ 2$) sources. The main goal of VERA is to make a three-dimensional map of the Galaxy and to reveal the velocity field of the Galactic rotation. VERA is currently observing H_2O and SiO masers associated with evolved stars and young stellar objects distributed in the whole Galaxy. The first results of VERA astrometric observations have shown the high capability of annual parallax and 3-D motion measurements on the scale of the Galaxy (e.g., Honma et al. 2007).

The revealed 3-D velocity field should reflect the mass distribution of the Galaxy. In order to derive the surface density of the gravitating matter in the Galactic disk as a function of hight from the Galactic plane, z, one can use a distribution of stars and a velocity dispersion in the direction perpendicular to the Galactic plane. The stellar population for the velocity field measurements has to be old because they should converge into dynamical equilibrium in the Galactic potential. Because Mira variables are long-lived stars, we can expect that they have been dynamically relaxed. VERA will continue astrometric observations of the Galactic Miras, which will provide information in detail on the vertical structure and gravitational potential within a size up to the Galaxy scale.

It is well known that there is a relation between the pulsation periods and luminosities (PL relation) of Mira variables, and this relation is used as a distance estimator for the Galactic stars or nearby galaxies. The PL relation of Mira variables has been studied using the variables in the Large Magellanic Cloud (LMC). Feast et al. (1989) showed the PL relation for 55 Mira variables in LMC. In order to obtain a Mira PL relation

in the Galaxy, it is necessary to measure the distances to individual stars. Although the Hipparcos satellite measured the positions, distances, and proper motions of ~ 100000 stars with a positional accuracy of 2 milliarcsecond (mas), these stars are located within only a few hundred parsecs from the Sun (Perryman et al. 1997). Because of the limited number of Mira variables in the solar neighborhood, the PL relation of the Galactic Mira variables has not yet been established as clearly as the relation in LMC. Although Whitelock, Feast, and van Leeuwen (2008) took advantage of the new analysis of the Hipparcos data (van Leeuwen 2007a), the target volume is much smaller than the whole size of the Galaxy. Galactic-scale astrometry being taken advantage of, VERA will offer a significant improvement to derive the PL relation for asymptotic giant branch (AGB) variables in the Galaxy in the near future.

In this paper, we show results of phase-referencing observations of H_2O masers toward SY Sculptoris (SY Scl) with VERA. These observations have been conducted as one of the primary scientific projects of VERA: measurements of annual parallaxes of the Galactic Mira variables to establish the PL relation in the Galaxy. SY Scl is an AGB star classified as a Mira variable with a pulsation period of 415 d (Whitelock et al. 1994). The effective temperature is estimated to be 2200–2400 K based on the spectral type of M8e (Hansen & Blanco 1975). The distance from the Sun to SY Scl was estimated to be 1.45 kpc using the PL relation for oxygen-rich (O-rich) Mira variables found in LMC (Feast 1996; Feast & Whitelock 2000; van Leeuwen 2007b). SY Scl is one of the stars suitable for establishing the PL relation and revealing 3D kinematics in the solar neighborhood.

2. Observations and Data Analysis

The VERA observations have been made with the four antennas located at Mizusawa, Iriki, Ogasawara, and Ishigakijima at 11 epochs with a typical duration of 5–6 hr. Table 1 summarizes the observations. At each epoch, the H_2O $6_{16}-5_{23}$ maser line at a rest frequency of 22.235080 GHz toward SY Scl [$\alpha = 00^{\rm h}07^{\rm m}36\overset{\rm s}{.}24756$, $\delta = -25°29'40\overset{''}{.}02813$(J2000.0)] and the continuum emission from J0011−2612 [$\alpha = 00^{\rm h}11^{\rm m}01\overset{\rm s}{.}246737$, $\delta = -26°12'33\overset{''}{.}37684$(J2000.0)] (Fey et al. 2004) were observed simultaneously with the dual-beam system of VERA. The instrumental phase delay between two signal paths was recorded during the observations (Kawaguchi et al. 2000). The continuum source, J0011−2612, separated from SY Scl by $1\overset{\circ}{.}05$, was observed as a position reference and detected with a peak flux density of ~ 350 mJy. The data were recorded onto magnetic tapes at a rate of 1024 Mbps, yielding a total bandwidth of 256 MHz. This was separated into 16 IF channels, each with a bandwidth of 16 MHz. A single IF channel was assigned to SY Scl, and the remaining ones to J0011−2612. The recorded signals were correlated using the Mitaka FX correlator (Chikada et al. 1991). In the data of maser emission, the frequency and velocity resolutions are 15.625 kHz and 0.21 km s^{-1}, respectively. Since a delay-tracking model used in the calculation of a priori delays in the Mitaka FX correlator was not accurate enough for the astrometry with VERA, we have applied better estimates of a priori models obtained through the same procedure as was described in Nakagawa et al. (2008).

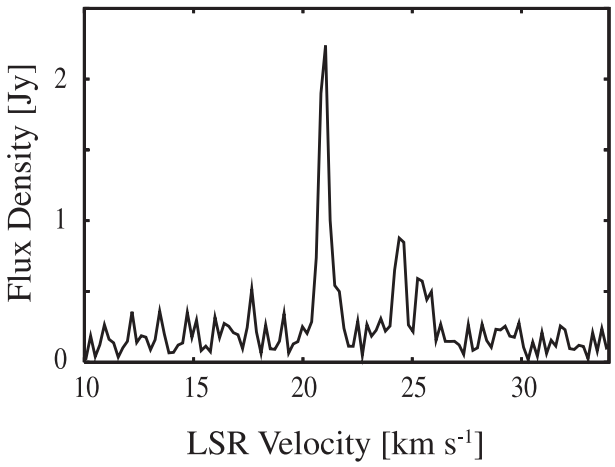

Fig. 1. Cross-power spectrum of H_2O maser emission of SY Scl observed with the VERA Mizusawa−Iriki baseline (1267 km) on 2008 February 21.

We used the NRAO Astronomical Image Processing System (AIPS) package for data analysis. The amplitude calibration was mainly performed by using system temperatures and antenna gains logged during the observations. Phase solutions from the fringe search process for J0011−2612 were transferred to the SY Scl data. Then, amplitude and phase solutions from self-calibration of J0011−2612 were also transferred to SY Scl. After these calibrations, we created image cubes of the H_2O masers, which had 512×512 pixels, each with a pixel size of 0.05 mas. The synthesized beam size was typically 1.8 mas $\times$ 1.1 mas with a position angle of 20°. At most of the epochs, the quality of phase-referenced maps was not high because of a limitation of the dynamic range of the image attributed to poor (u, v) coverage at a declination of −25° and the residual of wet atmospheric zenith delays (see subsection 4.1). In order to improve the image quality, we estimated the residual atmospheric zenith delay offset, using the image-optimization method (Honma et al. 2008). This correction was applied to one of the four stations of VERA, by which the coherence of the phase-referenced map was best improved. These residuals were then loaded into AIPS and applied in the same manner as the delay tracking correction. By Fourier-transforming these calibrated data, we obtained a phase-referenced map of SY Scl, and fitted it to a two-dimensional Gaussian model to find the position. These positions were used to derive the annual parallax and proper motions.

3. Results

3.1. Annual Parallax and Proper Motion

Figure 1 shows the H_2O maser spectrum of SY Scl obtained on 2008 February 21. The H_2O maser components at $V_{\rm LSR} = 21$ km s^{-1} and 25 km s^{-1} were detected at all observations. The two spectral components were resolved into several maser features. The component at $V_{\rm LSR} = 21$ km s^{-1} was typically 3 times as bright as that at 25 km s^{-1}, and contained maser

Table 1. Observation and detected masers.*

Epoch	Code	Date [YY/MM/DD]	Duration [UT]	Synthesized beam [mas × mas]	1σ-noise [Jy beam^{-1}]	N
1	r06302a	06/10/30	09:35–15:40	1.8 × 1.1, 22°	0.36	2
2	r07106b	07/04/16	22:35–04:55	1.6 × 1.0, 168°	0.09	4
3	r07314a	07/11/13	08:30–14:50	1.9 × 1.1, 6°	0.17	5
4	r07341b	07/12/07	07:00–13:20	1.9 × 1.3, 25°	0.32	2
5	r08019b	08/01/19	04:00–10:20	1.9 × 1.2, 31°	0.18	7
6	r08055a	08/02/24	01:30–07:50	1.9 × 1.2, 20°	0.19	5
7	r08101b	08/04/10	22:30–04:50	1.9 × 1.2, 152°	0.13	2
8	r08140b	08/05/19	20:25–02:45	1.8 × 1.5, 21°	0.32	3
9	r08177b	08/06/25	17:45–00:05	2.1 × 1.2, 150°	0.25	1
10	r08213b	08/07/31	16:00–22:00	2.0 × 1.3, 17°	0.41	2
11	r08240b	08/08/27	14:25–20:10	2.1 × 0.8, 172°	0.29	2

* Column (2) — Observation code with a form of rYYDDDx, where YY denotes the last two digits of the year, DDD is the day of year, x = a/b is a note to distinguish observations in the same day. Column (3) — Date (YY/MM/DD). Column (4) — Duration of the observation. Column (5) — Major- and minor-axis lengths and position angle of the synthesized beam. Column (6) — Noise level per velocity channel. Column (7) — Number of detected masers.

feature A. It has been used for measurement of the annual parallax and proper motion, because it has kept the highest flux density and was detected at 9 epochs during the observation period of 2 yr without structural change. Maser feature B was detected in only 3 observations. Other maser features were detected only in a few epochs (see table 2), and therefore it was difficult to use them in parallax measurements.

At first, we simultaneously determined the parallax, π, and proper motion, (μ_x, μ_y), using a least-squares fitting. We obtained an annual parallax of 0.71 ± 0.11 mas, corresponding to a distance of $1.41^{+0.12}_{-0.19}$ kpc. Secondly, we made the same analysis using only the data of right-ascension offsets to obtain better estimates of π and μ_x. Because SY Scl is located at a declination of $-25°$, significant impact on the astrometric result is expected from the tropospheric zenith delay residuals in the declination direction. Using right-ascension offsets, we obtained an annual parallax of 0.75 ± 0.03 mas and a proper motion, μ_x, of 6.41 ± 0.04 mas yr^{-1}. The measured parallax corresponds to a distance of 1.33 ± 0.05 kpc. After these solutions were derived, we estimated μ_y using the data of declination offsets. The proper motion, μ_y, was obtained to be -6.90 ± 0.12 mas yr^{-1}. The standard deviation of the data from the best-fit model was obtained to be (σ_x, σ_y) = (0.12, 0.36) [mas]. Figure 2 shows the positions of the masers (filled circle) and best-fit model (solid line).

3.2. H_2O Maser Distribution and Stellar Position

Figure 3 shows the H_2O maser distribution and the internal motions. The masers were found to be distributed within an area of 55 mas × 60 mas (70 AU × 80 AU at a distance of 1.33 kpc), in which the red-shifted and blue-shifted components are located on the NW and SE sides, respectively. The positions in figure 3 represent the offsets from the tracking center ($00^h07^m36^s.24756$, $-25°29'40''.02813$), and have an uncertainty of 0.22 mas in right ascension and 0.34 mas in declination; they mainly come from the position uncertainty of the reference source, J0011−2612 (Fey et al. 2004). For five maser features continuously detected at more than two observations, we traced their positions and detected relative motions with respect to the tracking center. Averaging these motions out, we obtained (6.82, −8.73) [mas yr^{-1}]. Then, subtracting it from the absolute motions of each maser, we derived internal motions of masers around SY Scl. Since there are only motions from a few components, here we assume that the average internal motions of all features are zero. We also note that this does not produce motions with respect to the star, but just with respect to the common mean. For five features, the typical transverse velocity was obtained to be 1 mas yr^{-1}, corresponding to 6 km s^{-1}. Table 2 summarizes the positions and kinematics of masers.

The positions of evolved stars in the circumstellar envelopes were estimated in several manners, mainly based on position–radial-velocity diagrams. For H_2O maser sources, it is more difficult to estimate a stellar position compared with SiO maser sources. SiO masers are located much closer to the central star than other maser species (Moran et al. 1979), or in the transition region between the stellar surface and the circumstellar envelope (Elitzur 1980; Nyman & Olofsson 1986). In addition, they often exhibit ring morphology, whose center may coincide with the stellar position. Bowers, Claussen, and Johnston (1993) assumed that a star is located at the center of the H_2O maser distribution, or at the middle point between the red-shifted and blue-shifted maser features. Based on this assumption, a middle point between the most red-shifted feature B and the most blue-shifted one, G, is chosen as a stellar position, and is indicated by a cross symbol at (-9.9 ± 0.1, 3.0 ± 0.1) [mas] in figure 3. We also estimated the stellar position and velocity using a model-fitting analysis that was almost the same as those adopted in previous works (Genzel et al. 1981; Reid et al. 1988; Gwinn et al. 1992; Imai et al. 2000). This method involves an assumption that each velocity vector is in the radial direction from the originating point of expanding outflow. Using the measured proper motions of maser features A to E, we obtained a stellar position of (-10.2 ± 15.1, 0.0 ± 7.7) [mas], which is indicated by a plus symbol with error bars. We also obtained a stellar systemic radial velocity of 22 km s^{-1}. The stellar

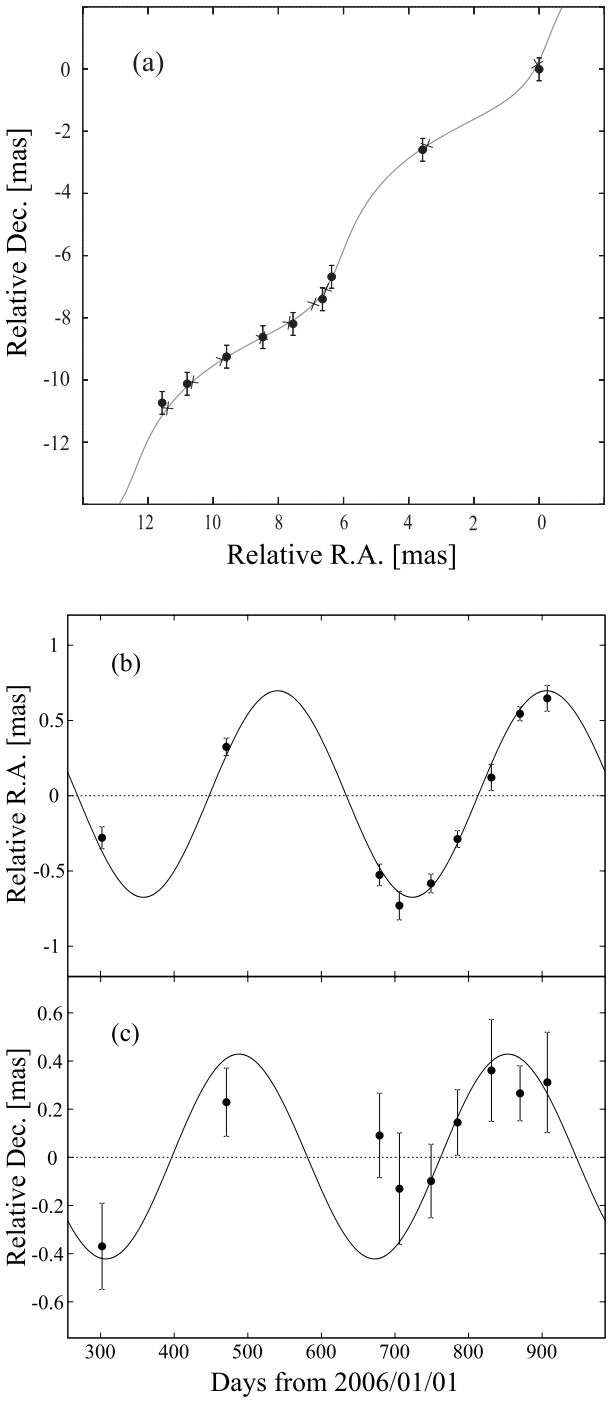

Fig. 2. Motion of H_2O maser feature A. The position offsets from that on 2006 October 30 are displayed. (a) Motion of feature A on the sky. A filled circle indicates the measured maser position and a cross indicates the position predicted from a model. A gray solid curve shows the fitted motion composed of a parallactic motion and a linear proper motion. (b) Oscillation along right ascension due to the annual parallax. We obtained it by subtracting the proper motion from the observed motion. (c) Same as (b), except for declination.

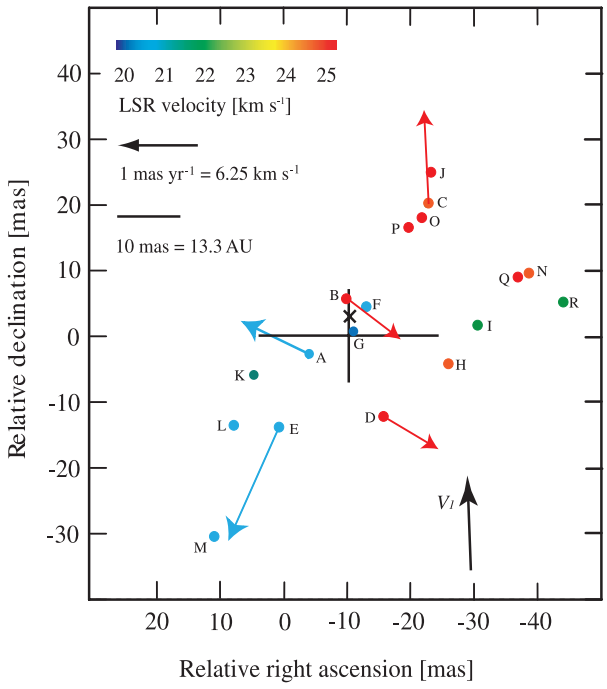

Fig. 3. Distribution of H_2O maser features around SY Scl. Filled circles show H_2O masers. A color bar at the top-left corner denotes the radial velocity of the feature. A root of an arrow indicates the location of the maser at its first detection. The length and direction of an arrow indicate the velocity and direction of the maser proper motion. An arrow at the top-left corner illustrates a proper motion of 1 mas yr^{-1}, corresponding to 6.25 km s^{-1} at the source distance of 1.33 kpc. The cross and plus symbols indicate the stellar positions estimated from two different techniques (see the main text). The arrow V_1 indicates the eigenvector with the largest eigenvalue in the diagonalized VVCM (see the main text), indicating the major axis of the maser motions.

positions estimated from two methods coincide with each other within a few mas.

3.3. *Systemic Motion of SY Scl*

We derived an SY Scl's systemic motion of $(\mu_x^\star,\ \mu_y^\star) = (5.57 \pm 0.04,\ -7.32 \pm 0.12)$ [mas yr^{-1}] from the motion of maser feature A (μ_x, μ_y), subtracting its internal motion. Using the source Galactic coordinates of $(l,\ b) = (39.^\circ91,\ -80.^\circ05)$, we obtained that the systemic motion in Galactic coordinates is $(\mu_l^\star,\ \mu_b^\star) = (-6.13 \pm 0.04,\ -6.86 \pm 0.08)$ [mas yr^{-1}], corresponding to a velocity vector of $(v_l^\star, v_b^\star) = (-38.5 \pm 0.3,\ -43.1 \pm 0.5)$ [km s^{-1}] at the source distance of 1.33 kpc. The systemic motion is converted to that with respect to the Local Standard of Rest (LSR), by adopting a solar motion of $(U_\odot,\ V_\odot,\ W_\odot) = (10.0 \pm 0.4,\ 5.2 \pm 0.6,\ 7.2 \pm 0.4)$ [km s^{-1}] (Dehnen & Binney 1998b). Here, U points to the Galactic center, V in the direction of the Galactic rotation, and W to the northern Galactic pole. Using the stellar radial velocity of 22 km s^{-1}, we found that the star has a motion of $(U_s,\ V_s,\ W_s) = (-5.2 \pm 0.3,\ -53.8 \pm 2.1,\ -33.3 \pm 0.3)$ [km s^{-1}] with respect to the LSR. We can see that SY Scl moves approximately south from the Galactic plane with a peculiar velocity of 63 ± 2 km s^{-1}.

Table 2. Parameters of H_2O masers in SY Scl.*

ID	V_{LSR} [km s^{-1}]	RA offset [mas]	Dec offset [mas]	Flux [Jy beam^{-1}]	v_x [mas yr^{-1}]	v_y [mas yr^{-1}]	Epoch ID when detected
A	20.9	−4.70(0.06)	−1.90(0.08)	3.76(0.56)	0.84	0.42	123456789**
B	25.7	−9.91(0.04)	5.62(0.09)	0.70(0.14)	−0.76	−0.60	**345******
C	24.5	−22.65(0.05)	20.36(0.11)	0.45(0.12)	0.10	1.47	*23*5******
D	25.3	−14.41(0.07)	−14.40(0.13)	0.67(0.15)	−0.75	0.01	**3*56*****
E	20.9	0.83(0.06)	−14.72(0.05)	0.63(0.16)	0.58	−1.30	**3*56*****
F	20.7	−13.06(0.03)	4.68(0.12)	1.92(0.41)	—	—	*******8*10*
G	20.5	−9.95(0.06)	0.43(0.14)	2.01(0.50)	—	—	*******8*10*
H	24.5	−26.01(0.05)	−4.51(0.10)	0.52(0.04)	—	—	1**********
I	22.4	−30.65(0.07)	1.74(0.11)	0.34(0.11)	—	—	*2*********
J	25.7	−23.14(0.09)	25.03(0.15)	0.34(0.12)	—	—	*2*********
K	21.5	4.43(0.04)	−6.23(0.08)	0.56(0.09)	—	—	****5******
L	20.7	8.11(0.05)	−13.80(0.11)	0.95(0.20)	—	—	****5******
M	20.9	10.91(0.03)	−30.59(0.18)	1.29(0.30)	—	—	******7****
N	24.7	−39.10(0.04)	9.80(0.13)	0.45(0.10)	—	—	**********11
O	24.9	−21.02(0.06)	18.09(0.14)	0.41(0.09)	—	—	*****6*****
P	24.7	−18.90(0.05)	16.60(0.06)	0.76(0.20)	—	—	*****6*****
Q	25.3	−37.90(0.04)	9.51(0.09)	0.40(0.11)	—	—	**********11
R	22.6	−44.71(0.07)	5.08(0.10)	0.45(0.18)	—	—	**3********

* Column (1)—Component ID. Column (2)—LSR velocity in km s^{-1}. Column (3)—Position offsets in RA relative to the tracking center. Column (4)—Position offsets in Dec relative to the tracking center. Column (5)—Brightness of the feature at the first detection in Jy beam^{-1}. Column (6), (7)—Best fit linear motion in RA and Dec in mas yr^{-1}, respectively. Column (8)—Epoch ID of successful maser detection. Numbers in parenthesis represent the uncertainties.

4. Discussion

4.1. Astrometric Error Sources

In this section, we discuss the astrometric position error of our measurement by considering possible error factors. In our analysis of the parallax and proper motion, the standard deviation of the data from the best-fit model was obtained to be $(\sigma_x, \sigma_y) = (0.12, 0.36)$ [mas]. We choose these deviations as position errors of our measurement.

Firstly, we consider that an error depends on the signal-to-noise ratio (R_{SN}) of the phase-referenced images. In our observations, the typical R_{SN} of images is 6 to 12. Using the beam size (θ_b) and R_{SN}, the maximum error contribution (θ_b/R_{SN}) can be estimated to be 100 μas in right ascension and 280 μas in declination. Secondly, we estimate an error caused by residuals of the tropospheric zenith delay. Honma et al. (2007) and Nakagawa et al. (2008) indicate that the typical tropospheric zenith delay residual is 3 cm. Based on their studies, we estimate the position error to be 50–150 μas. In this estimation, 1.°05 is used as a separation angle of SY Scl and the reference source J0011−2612. Refer to subsection 4.1 of Honma et al. (2007) for further details of this procedure. Thirdly, we considered station-position errors and realized that this factor is one order of magnitude smaller than that from the tropospheric zenith delay residual (Honma et al. 2007). This is not likely to be the main source of observation errors. Next, we consider an effect caused by the position uncertainty of the reference source J0011−2612. The position uncertainty of this source is (0.22, 0.34) [mas] (Fey et al. 2004). During our observations, this source exhibited a pointlike structure with no structural variation, and we do not think that this effect is serious. Then, finally we mention a variation of the internal structure of the masers (e.g., Hirota et al. 2008). In our observation, the maser feature A that has been used in our astrometric measurements has not shown any clear structural change. However, we cannot rule out this possibility concerning the present work. Under the assumption that the quadratic sum of each error factor explains the largest observation error, $\sigma_y = 0.36$ mas, we find 170 μas to be the position uncertainty due to a structural effect of the maser. Sometimes, maser emission shows a complicated structure as large as a few milliarcseconds, 170 μas, which is one order smaller than that of the structure, is acceptable as an error derived from the structural effect.

Therefore, we argue that the residuals in the measurement are understood, and can be attributed to the limitation of the image dynamic range, atmospheric zenith delay residuals, and the maser structure.

4.2. The Orbit of SY Scl in the Galaxy

We found a peculiar motion of the star with respect to LSR, $(U_s, V_s, W_s) = (-5.2 \pm 0.3, -53.8 \pm 2.1, -33.3 \pm 0.3)$ [km s^{-1}]. To see the orbit of SY Scl and consider its kinematics in the Galaxy, we performed a calculation for the last 1 Gyr using a 4th-order Runge-Kutta method with a time step of 0.01 Myr. Since a typical time scale of the Galactic rotation near the Sun is on the order of 10^8 yr ($\sim 2\pi R_0/V_0$), 1 Gyr is fit for showing the orbits and realizing the difference in orbit. In addition, since the Galactic Mira variables with periods of 370–660 d have ages of at least 1.3 Gyr (Feast et al. 2006; Feast 2009), it is reasonable to use 1 Gyr in this calculation. We adopted a parameterized model of the mass distribution within the Galaxy (Dehnen & Binney 1998a). In this model, the distance

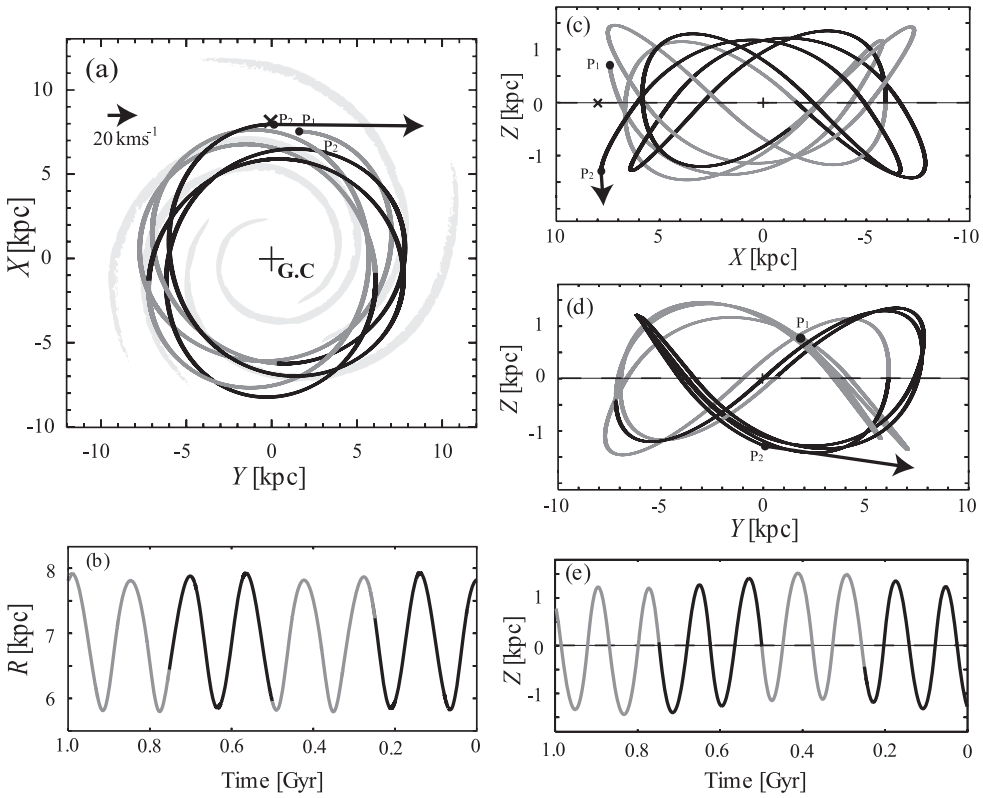

Fig. 4. Orbit of SY Scl for the last 1 Gyr on the schematic view of the Galaxy. The black and gray solid line indicates the orbit of SY Scl over 1 Gyr in which the colors are changed every 250 Myr. (a) Orbit in the face-on view of the Galaxy. P_1 and P_2 indicate the positions of SY Scl 1 Gyr ago and at present, respectively. A cross indicates the Sun's location $(X_\odot, Y_\odot, Z_\odot) = (8.0, 0, 0)$ [kpc]. Spiral arms are depicted using the result from Nakanishi and Sofue (2006). (b) Time variation of radial distance from the Galactic center. (c) Orbit in the edge-on view (X–Z plane). (d) Same as (c) but in the Y–Z plane. (e) Time variation of distance from the Galactic plane. Dashed lines in (c), (d), and (e) represent the Galactic plane ($Z = 0$).

from the Galactic center to the Sun, $R_0 = 8.0$ kpc, a scale length of the exponential disk, $R_\mathrm{d} = 2.4$ kpc, and a circular velocity at the solar circle, $V_0 = 217.4\,\mathrm{km\,s^{-1}}$, were adopted. The Galactic potential is axisymmetric, and thus does not account for the minor deviation in the potential field near the spiral arms, or for any evolution of the potential field. In the Cartesian coordinate system, the position and space motion at present are expressed as $(X, Y, Z) = (7.8, 0.1, -1.3)$ [kpc] and $(V_R, V_\theta, V_Z) = (-1.8^{+0.6}_{-0.6}, 178.5^{+2.3}_{-2.1}, -25.9^{+0.3}_{-0.3})$ [$\mathrm{km\,s^{-1}}$], respectively, where X is the position measured along the axis to the anti-Galactic center, Y in the direction of Galactic rotation, and Z to the north Galactic pole. Figure 4 illustrates the orbit of SY Scl in the (X, Y, Z) coordinate system during the last 1 Gyr. One can see that the orbit shows large distortion and oscillation, compared with the Sun's orbit presented in Gies and Helsel (2005). The radial oscillation has a period of 142 Myr, and shows an amplitude of 1.1 kpc (figure 4 b). The orbit projected in the Z-direction has an amplitude of 1.5 kpc and its period is 120 Myr (figure 4e). Therefore, SY Scl apparently orbits as a member of the Galactic thick disk rather than a thin disk.

4.3. Comparison with the Period–Luminosity Relation

AGB stars are important distance indicators for old- and intermediate-age populations. They are luminous both in all wavelengths and in the near infrared, and are easily identified by their late spectral types, amplitudes, and periods of the stellar pulsation.

Using sources with well-estimated distances, Whitelock, Feast, and van Leeuwen (2008) presents the PL relation for Galactic AGB variables. Parallax measurements from VLBI astrometric observations (Vlemmings et al. 2003; Kurayama et al. 2005; Vlemmings & van Langevelde 2007) were used in the study. If we apply the SY Scl pulsation period of 415 d to the PL relation in Whitelock, Feast, and van Leeuwen (2008), we obtain an absolute K magnitude of $M_K = -8.09 \pm 0.07$ mag. The error of M_K comes from a zero-point error. Based on our distance measurement of 1.33 ± 0.05 kpc and the apparent K magnitude, $m_K = 2.54$ mag (Whitelock et al. 1994), we obtain the absolute K magnitude $M_K = -8.07 \pm 0.08$ mag. These two estimates are approximately consistent, and thus we found no discrepancy between the Galactic PL relation in Whitelock, Feast, and van Leeuwen (2008) and our distance measurement.

4.4. Maser Feature Distribution

From the internal motions of maser features around SY Scl, we discuss the spatio-kinematic structure of the masers. In our observation, the proper motions of only 5 maser features were detected. Under the assumption that the stellar position

is reflected by the average, these maser features have a radial expansion velocity of $V_{\rm exp} = 5$–$9\,{\rm km\,s^{-1}}$. Since all of the highly collimated bipolar outflows observed in evolved stars show a large expansion velocity of $\geq 30\,{\rm km\,s^{-1}}$ (e.g., Imai et al. 2002), a bipolar outflow model may not be accepted in the case of SY Scl.

We extracted kinematic essentials in a fully objective manner without assuming any particular model. We used an analytic tool based on diagonalization of the velocity variance/covariance matrix (VVCM) (Bloemhof 1993), which is composed of the following elements:

$$\sigma_{ij} = \frac{1}{N-1}\sum_{n}^{N}(v_{i,n} - \overline{v_i})(v_{j,n} - \overline{v_j}), \quad (1)$$

where i and j denote three orthogonal space axes; n is the n-th maser feature in a collection totaling $N(=5)$. The diagonal elements are just the velocity dispersions along the three Cartesian axes. The VVCM was initially evaluated in a coordinate system with axes along right ascension, declination, and radial direction increasing toward the target source. The matrix was diagonalized as follows (in units of ${\rm km^2\,s^{-2}}$):

$$\begin{pmatrix} 21.4 & 1.8 & -10.3 \\ 1.8 & 42.9 & 3.9 \\ -10.3 & 3.9 & 5.7 \end{pmatrix} \Rightarrow \begin{pmatrix} 43.3 & 0 & 0 \\ 0 & 26.5 & 0 \\ 0 & 0 & 0.1 \end{pmatrix}. \quad (2)$$

The eigenvector for the largest eigenvalue indicates the major axis of the outflow. The largest eigenvalue is larger than the second largest one by a factor of only 1.6. The eigenvector V_1 with the larger eigenvalue has a PA of 2° with a inclination angle of −5° with respect to the sky plane. Although the number of masers included in this consideration is small, our analysis shows the motions to be consistent with expansion motion in a single plane, possibly an equatorial wind.

4.5. Luminosity and Photosphere Radius

H_2O masers around Mira variables are typically distributed with radii ranging from 5 to 50 AU (Bowers & Johnston 1994). Here, we estimate the photosphere size of the central star and compare it with the size of the maser distribution. Le Bertre et al. (1998) found the luminosity of SY Scl to be $8.7 \times 10^3\,L_\odot$ based on a distance of 1.45 kpc, which was obtained using the PL relation of Mira variables in LMC. Here, we reestimate the stellar luminosity using a distance more accurately derived from our parallax measurement. Considering a difference between two distances, 1.45 kpc and 1.33 kpc, we reestimate the stellar luminosity to be $7.3 \times 10^3\,L_\odot$. Then, assuming it to be blackbody radiation we obtain an SY Scl photosphere radius of 2.5 AU. Here, we have chosen 2200–2400 K as an effective temperature that comes from the spectral type of M8e (Hansen & Blanco 1975). The maser features in SY Scl were found to be distributed in an area of 70 AU × 80 AU, showing a typical distribution size of H_2O masers around Mira variables.

5. Conclusions

We determined that the annual parallax and systemic motion of SY Scl are $\pi = 0.75 \pm 0.03$ mas and $(\mu_x^\star, \mu_y^\star) = (5.57 \pm 0.04, -7.32 \pm 0.12)$ [mas yr^{-1}], respectively. The corresponding distance is 1.33 ± 0.05 kpc. At present, the star is located 1.3 kpc below the Galactic plane and moving further away from the Galactic plane. From the present position and motion, we calculated an SY Scl's orbit in the Galaxy based on a parametrized model for the Galactic gravitational potential. The period of the radial oscillation is ~ 142 Myr. The oscillation perpendicular to the Galactic plane has an amplitude of 1.5 kpc and a period of 120 Myr. We found that SY Scl is orbiting as a member of the Galactic thick disk stars.

Based on our determined distance, we found the absolute magnitude of SY Scl to be $M_K = -8.07 \pm 0.08$ mag. This value is consistent with -8.09 ± 0.07 mag, which was derived from the Galactic Mira PL relation in Whitelock, Feast, and van Leeuwen (2008) and the pulsation period of 415 d.

We used analytic tools based on diagonalization of the VVCM using the internal motions of H_2O masers. The masers seem to be moving along a plane slightly tilted from the sky plane. The derived luminosity and size of SY Scl's photosphere are $7.3 \times 10^3\ L_\odot$ and 2.5 AU, respectively, by the use of the luminosity data (Le Bertre et al. 1998), the effective temperature, $T_{\rm eff}$, and our measured distance. The masers in SY Scl were found to be distributed in an area of 70 AU × 80 AU, corresponding to 15 times as large as the stellar diameter.

To determine the mass distribution of the Galaxy, one needs to measure the spatial distribution and the velocity dispersion of such stars. SY Scl may have been a part of the dynamically relaxed distribution, and may be a star suitable for tracing the Galactic potential. This study presents an astrometric measurement for only one star, but demonstrates the high capability of VERA for studying the kinematic properties of individual stars harboring H_2O maser emission.

During the next decade, astrometric VLBI observations of hundreds of Galactic maser sources will provide information on the vertical structure and potential of the Galactic disk.

We thank Walter Dehnen for sending us his source code describing the Galactic gravitational potential.

References

Bloemhof, E. E. 1993, ApJ, 406, L75
Bowers, P. F., Claussen, M. J., & Johnston, K. J. 1993, AJ, 105, 284
Bowers, P. F., & Johnston, K. J. 1994, ApJS, 92, 189
Chikada, Y., Kawaguchi, N., Inoue, M., Morimoto, M., Kobayashi, H., & Mattori, S. 1991, in Frontiers of VLBI, ed. H. Hirabayashi et al. (Tokyo: Universal Academy Press), 79
Dehnen, W., & Binney, J. 1998a, MNRAS, 294, 429
Dehnen, W., & Binney, J. J. 1998b, MNRAS, 298, 387
Elitzur, M. 1980, ApJ, 240, 553
Feast, M. W. 1996, MNRAS, 278, 11
Feast, M. W. 2009, in Proc. AGB Stars and Related Phenomena, ed. T. Ueta et al. (Tokyo: National Astronomical Observatory of Japan), 48

Feast, M. W., Glass, I. S., Whitelock, P. A., & Catchpole, R. M. 1989, MNRAS, 241, 375
Feast, M. W., & Whitelock, P. A. 2000, MNRAS, 317, 460
Feast, M. W., Whitelock, P. A., & Menzies, J. W. 2006, MNRAS, 369, 791
Fey, A. L., et al. 2004, AJ, 127, 3587
Genzel, R., Reid, M. J., Moran, J. M., & Downes, D. 1981, ApJ, 244, 884
Gies, D. R., & Helsel, J. W. 2005, ApJ, 626, 844
Gwinn, C. R., Moran, J. M., & Reid, M. J. 1992, ApJ, 393, 149
Hansen, O. L., & Blanco, V. M. 1975, AJ, 80, 1011
Hirota, T., et al. 2008, PASJ, 60, 961
Honma, M., et al. 2007, PASJ, 59, 889
Honma, M., Tamura, Y., & Reid, M. J. 2008, PASJ, 60, 951
Imai, H., Kameya, O., Sasao, T., Miyoshi, M., Deguchi, S., Horiuchi, S., & Asaki, Y. 2000, ApJ, 538, 751
Imai, H., Obara, K., Diamond, P. J., Omodaka, T., & Sasao, T. 2002, Nature, 417, 829
Kawaguchi, N., Sasao, T., & Manabe, S. 2000, Proc. SPIE, 4015, 544
Kurayama, T., Sasao, T., & Kobayashi, H. 2005, ApJ, 627, L49
Le Bertre, T., Lagache, G., Mauron, N., Boulanger, F., Désert, F. X., Epchtein, N., & Le Sidaner, P. 1998, A&A, 335, 287
Moran, J. M., Ball, J. A., Predmore, C. R., Lane, A. P., Huguenin, G. R., Reid, M. J., & Hansen, S. S. 1979, ApJ, 231, L67
Nakagawa, A., et al. 2008, PASJ, 60, 1013
Nakanishi, H., & Sofue, Y. 2006, PASJ, 58, 847
Nyman, L.-A., & Olofsson, H. 1986, A&A, 158, 67
Perryman, M. A. C., et al. 1997, A&A, 323, L49
Reid, M. J., Schneps, M. H., Moran, J. M., Gwinn, C. R., Genzel, R., Downes, D., & Roennaeng, B. 1988, ApJ, 330, 809
Rygl, K. L. J., Brunthaler, A., Reid, M. J., Menten, K. M., van Langevelde, H. J., & Xu, Y. 2010, A&A, 511, A2
Shapiro, I. I., et al. 1979, AJ, 84, 1459
van Langevelde, H. J., Vlemmings, W., Diamond, P. J., Baudry, A., & Beasley, A. J. 2000, A&A, 357, 945
van Leeuwen, F. 2007a, Hipparcos, the New Reduction of the Raw Data (Dordrecht: Springer), 350
van Leeuwen, F. 2007b, A&A, 474, 653
Vlemmings, W. H. T., & van Langevelde, H. J. 2007, A&A, 472, 547
Vlemmings, W. H. T., van Langevelde, H. J., Diamond, P. J., Habing, H. J., & Schilizzi, R. T. 2003, A&A, 407, 213
Whitelock, P. A., Feast, M. W., & van Leeuwen, F. 2008, MNRAS, 386, 313
Whitelock, P., Menzies, J., Feast, M., Marang, F., Carter, B., Roberts, G., Catchpole, R., & Chapman, J. 1994, MNRAS, 267, 711